European Journal of Pharmaceutics and Biopharmaceutics 134 (2019) 37–48

Contents lists available at ScienceDirect

European Journal of Pharmaceutics and Biopharmaceutics

journal homepage: www.elsevier.com/locate/ejpb

Research paper

Comparative evaluation of dimeric and monomeric forms of ADAPT scaffold protein for targeting of HER2-expressing tumours

Javad Garousi[a,1], Sarah Lindbo[b,1], Jesper Borin[b], Emma von Witting[b], Anzhelika Vorobyeva[a], Maryam Oroujeni[a], Bogdan Mitran[c], Anna Orlova[c], Jos Buijs[a], Vladimir Tolmachev[a,*], Sophia Hober[b]

[a] Department of Immunology, Genetics and Pathology, Uppsala University, SE-75185 Uppsala, Sweden
[b] Department of Protein Technology, KTH – Royal Institute of Technology, SE-10691 Stockholm, Sweden
[c] Department of Medicinal Chemistry, Uppsala University, Uppsala, Sweden

ARTICLE INFO

Keywords:
ADAPT
HER2
Dimer
Radionuclide molecular imaging
Indium-111
Iodine-125

ABSTRACT

ADAPTs are small engineered non-immunoglobulin scaffold proteins, which have demonstrated very promising features as vectors for radionuclide tumour targeting. Radionuclide imaging of human epidermal growth factor 2 (HER2) expression *in vivo* might be used for stratification of patients for HER2-targeting therapies. ADAPT6, which specifically binds to HER2, has earlier been shown to have very promising features for *in vivo* targeting of HER2 expressing tumours. In this study we tested the hypothesis that dimerization of ADAPT6 would increase the apparent affinity to HER2 and accordingly improve tumour targeting. To find an optimal molecular design of dimers, a series of ADAPT dimers with different linkers, -SSSG- (DiADAPT6L1), -$(SSSG)_2$- (DiADAPT6L2), and -$(SSSG)_3$- (DiADAPT6L3) was evaluated. Dimers in combination with optimal linker lengths demonstrated increased apparent affinity to HER2. The best variants, DiADAPT6L2 and DiADAPT6L3 were site-specifically labelled with ^{111}In and ^{125}I, and compared with a monomeric ADAPT6 in mice bearing HER2-expressing tumours. Despite higher affinity, both dimers had lower tumour uptake and lower tumour-to-organ ratios compared to the monomer. We conclude that improved affinity of a dimeric form of ADAPT does not compensate the disadvantage of increased size. Therefore, increase of affinity should be obtained by affinity maturation and not by dimerization.

1. Introduction

Molecular recognition of cancer-associated alterations, i.e. targeting, is one of the most promising strategies in treatment of disseminated malignancies. Specific molecular recognition can be used for delivery of cytotoxic drugs and for blocking of receptors/ligands involved in mitotic signalling or inhibition of immune checkpoints. One of the obstacles for efficient application of this strategy is an inter- and intrapatient heterogeneity of expression of molecular targets. Patients with tumours, which do not express specific targets, would not benefit from targeted therapy but might instead suffer from treatment-associated side effects. Radionuclide molecular imaging of therapeutic targets *in vivo* is a non-invasive means to enable selection of patients, who have tumours with homogenously expressed molecular targets and therefore would respond to a particular therapy [1].

Success of companion diagnostics depends on sensitivity and specificity of imaging, which in turn depends on the biodistribution and targeting properties of the imaging probes. One of the most promising approaches to improved sensitivity and specificity is the use of small targeting probes, based on single domain antibodies and engineered non-immunoglobulin scaffold proteins [2]. Due to their small size, such probes provide specific localization of a radionuclide in tumours within 30 min, and unbound tracers are rapidly cleared through kidneys. This enables imaging with a high contrast and sensitivity at the day of administration. In addition, small proteins do not accumulate in tumours due to the enhanced permeability and retention (EPR) effect [3], which increases specificity of imaging in comparison with imaging mediated by radiolabelled monoclonal antibodies.

We have recently reported development of a novel type of imaging probe based on the scaffold of the albumin binding domain (ABD) of streptococcal protein G. A dedicated binding site was created in ABD by construction of a combinatorial library through randomization of

* Corresponding author.
E-mail address: vladimir.tolmachev@igp.uu.se (V. Tolmachev).
[1] Contributed equally.

https://doi.org/10.1016/j.ejpb.2018.11.004
Received 23 August 2018; Received in revised form 19 October 2018; Accepted 4 November 2018
Available online 05 November 2018

A

DiADAPT6L1: GVDANSLAAAKETALYHLDRLGVADAYKDLIDKAKTVEGVKARYFEILHALP-SSSG-LAAAKETALYHLDRLGVADAYKDLIDKAKTVEGVKARYFEILHALP-GSSC

DiADAPT6L2: GVDANSLAAAKETALYHLDRLGVADAYKDLIDKAKTVEGVKARYFEILHALP-SSSG-SSSG-LAAAKETALYHLDRLGVADAYKDLIDKAKTVEGVKARYFEILHALP-GSSC

DiADAPT6L3: GVDANSLAAAKETALYHLDRLGVADAYKDLIDKAKTVEGVKARYFEILHALP-SSSG-SSSG-SSSG-LAAAKETALYHLDRLGVADAYKDLIDKAKTVEGVKARYFEILHALP-GSSC

Monomer: GHEHEHEDANSLAAAKETALYHLDRLGVADAYKDLIDKAKTVEGVKARYFEILHALP-GSSC

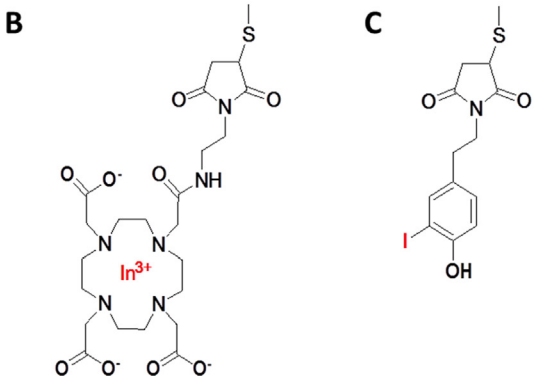

Fig. 1. A. Sequences of the dimeric ADAPT6 variants evaluated in this study, DiADAPT6L1, DiADAPT6L2, and DiADAPT6L3 as well as the sequence of $(HE)_3$DANS-ADAPT6-GSSC used as a monomeric comparator. Linkers are marked in red font, and the N-terminal amino acid sequence in blue font. Structures of maleimido-DOTA (B), and iodo-HPEM (C) conjugated to cysteine.

surface exposed amino acids. This library is enabling selection of binders with desired molecular specificity. Protein domains derived from this library are denoted ADAPTs [4]. ADAPTs with affinity in the low nanomolar range to cancer-associated targets such as tumour necrosis factor-α (TNF-α) [5], human epidermal growth factor receptor 3 (HER3) [6], and human epidermal growth factor receptor 2 (HER2) [7] have been selected. To facilitate blood clearance, the amino acids providing binding to albumin were replaced in an anti-HER2 ADAPT variant denoted ADAPT6 [7,8]. Feasibility of *in vivo* imaging of HER2 expression in tumours using ADAPT6 has been demonstrated [8]. HER2 is overexpressed in a substantial fraction of breast and gastro-oesophageal carcinomas and is clinically used as a molecular target for antibody- and tyrosine kinase inhibitors-based therapeutics [9,10]. Testing of HER2 expression levels in tumours is required to stratify patients for such therapies [11,12]. Radionuclide molecular imaging of HER2 expression offers the advantage of being non-invasive, which allows evaluation of the expression level repeatedly [13]. In further studies, the influence of histidine-containing tags [14], N- and C-terminal composition [15,16], position and residualizing properties of the radionuclide label [17] on biodistribution properties of ADAPT6 was evaluated. Based on these studies, an optimized variant of ADAPT6, $(HE)_3$DANS-ADAPT6-GSSC-DOTA was developed [18]. This variant provided several-fold better contrast to metastatic sites such as liver and bone compared to the parental variant [18].

It has to be noted that the existing variants of ADAPT6 have affinity to HER2 in the range of 1.2–4 nM, as measured using surface plasmon resonance (SPR). This level of affinity is sufficient for imaging of targets with high expression levels, ca. 10^6 receptors per cell, such as expression of HER2 in breast cancer (3+ according to HercepTest) [19]. However, a much more modest overexpression levels might also have a diagnostic value. For example, a HER2 expression of 1+ level (HercepTest) has a prognostic significance in prostate cancer [20]. This level of expression corresponds to 2–6 × 10^4 receptors per cell [21]. Expression levels of 20–50 thousands receptors per cell are typical for overexpressed IGF-1R [22,23], or HER3 [24]. Experience with another scaffold protein, the affibody molecule, suggests that subnanomolar affinity is required for imaging of targets with such expression levels [19].

Affinity of engineered scaffold proteins to desirable targets might be improved by affinity maturation [5,25,26]. An alternative to this lengthy process is dimerization of the binding modules. Dimerization may increase the apparent affinity by one order of magnitude by decreasing the off-rate. Therefore, the dimerization approach has been applied for improving targeting of a broad range of polypeptide binders, including short RGD peptides [27,28], exendin [29] and single-chain Fv fragments [30]. Another example is dimerization of the anti-HER2 affibody molecule ZHER2:4, which increased the affinity from 50 to 3 nM [31]. However, the effect of dimerization cannot be predicted straightforwardly. For example, dimerization of the anti-EGFR affibody molecule ZEGFR:1907 resulted in a less than two-fold increase of affinity, most likely due to steric hindrance of the binding interface in the C-terminal monomeric unit [32]. The issue of steric hindrance has also been documented for other targeting systems. For example, fusion of a toxin payload at the N- or C-terminus of targeting scFv resulted in a ten-fold difference of affinity of resulting immunotoxins [33]. Dimerisation of anti-CD20 single-domain antibody fragments (sdAb) αCD20 using a short G_4S linker resulted in an increased internalization of the construct by lymphoma cells, but the apparent affinity decreased slightly (from 2.9 ± 0.5 to 5.9 ± 1.9 nM)[34]. This prompts a careful optimization of the molecular design of dimeric ADAPTs. Furthermore, increase of hydrodynamic radius of a protein might complicate its extravasation into tumours.

The goal of this study was to find an optimal design of a dimeric anti-HER2 ADAPT6 and also to compare the *in vivo* targeting properties of monomeric and dimeric forms of ADAPT6. For dimerization, a variant having an N-terminal sequence containing the amino acids GVDANS was used. We selected this variant because (1) it has the smallest molecular weight with preserved stability of the scaffold [15] and (2) it has one of the most favourable biodistribution profiles (low uptake in blood and normal tissues) in its monomeric form [15]. In order to fuse two functional domains together but prevent mutual steric hindrance of binding, linkers built by small, flexible and uncharged amino acids are normally used. The most common versions are based on glycines and serines [35,36]. In this study, we selected a linker design that decreases the hydrophobicity of the constructs, since that would increase the liver uptake and/or hepatobiliary excretion of the

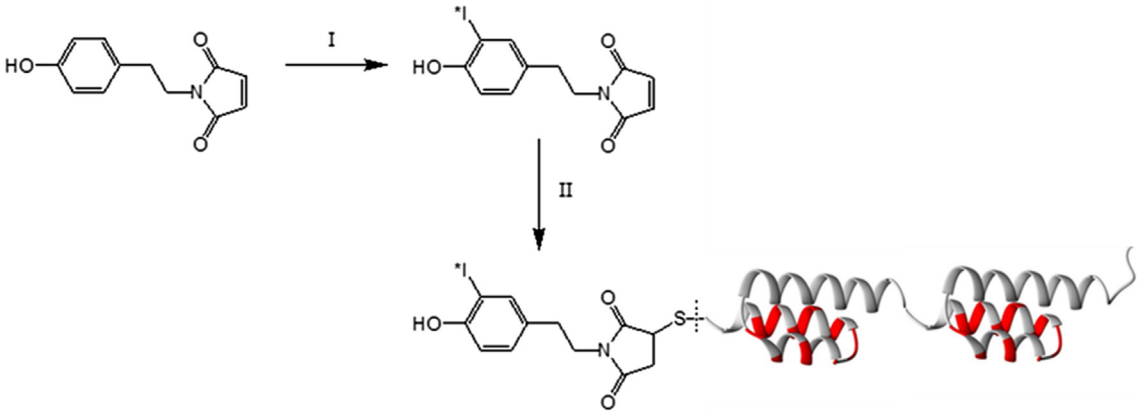

Fig. 2. Scheme of indirect radioiodination of DiADAPT6s using HPEM: I: ^{125}I-NaI in MeOH/HOAc; Chloramine-T; 5 min at room temperature; $Na_2S_2O_5$; II: freshly reduced DiADAPT6; pH 6.0, 60 min at room temperature.

constructs [37]. Hence, three serines and one glycine (SSSG) were chosen for construction of the linker region. Variant having one, two or three SSSG linker repeats were designated as DiADAPT6L1, DiADAPT6L2, and DiADAPT6L3, respectively (Fig. 1A). For site-specific labelling, a unique cysteine was introduced at the C-terminus of the three constructs. Previous studies demonstrated that placement of a label at the C-terminus of ADAPT6 provides the lowest uptake in normal tissues [16]. For labelling with residualizing radiometals, the versatile DOTA chelator was conjugated to the constructs using maleimide cysteine coupling (Fig. 1B). The non-residualizing radiohalogen label ^{125}I, was coupled to the dimeric constructs through an indirect radioiodination using ((4-hydroxyphenyl)ethyl)maleimide (HPEM) [16,38] (Fig. 2).

The constructs were produced and purified and their identity was confirmed by mass spectrometry. Thermal stability and re-folding fidelity were studied by circular dichroism spectra measurement under variable temperatures. The strength of binding to HER2 was measured by surface plasmon resonance. Efficacy and stability of labelling using ^{111}In and ^{125}I was evaluated. Binding specificity and affinity of binding to HER2-expressing cancer cell lines and cellular processing of conjugates after binding was evaluated *in vitro*. Specificity of HER2 binding *in vivo* and tumour-targeting properties of the most promising dimeric forms were studied in nude mice bearing human HER2-expressing xenografts and compared with the best monomeric variant, $(HE)_3$DANS-ADAPT6-GSSC, which was labelled in the same way.

2. Materials and methods

$^{111}InCl_3$ was purchased from Mallinckrodt Sweden AB (Stockholm, Sweden). [^{125}I] sodium iodide was purchased from PerkinElmer (Waltham, MA). The synthesis and characterization of HPEM was done based on the method described by Mume and co-workers [39]. Buffers used for labelling were prepared from high-quality Milli-Q water and purified from metal contamination using Chelex 100 resin (Bio-Rad Laboratories, Hercules, CA).

The HER2-expressing ovarian cancer cell line SKOV-3 and breast cancer cell line BT-474 were used in the cell studies. Both cell lines were obtained from American Type Culture Collection (ATCC, Manassas, VA). Cells were cultured in RPMI medium supplemented with 10% fetal calf serum, 2 mM L-glutamine and PEST (penicillin 100 IU/ml and 100 μg/ml streptomycin).

An automated γ-spectrometer with a ~7.6-cm (3-in) NaI(Tl) detector (1480 WIZARD; Wallac Oy, Turku, Finland) was used to measure radioactivity.

Data on cellular uptake were analyzed by unpaired 2-tailed *t* test using GraphPad Prism (version 4.00 for Windows; GraphPad Software, San Diego, CA) to determine significant differences ($p < 0.05$). Analysis of biodistribution data obtained in dual-label experiments were performed using paired *t*-test. One-way ANOVA analysis with Bonferroni's multiple comparison test was used to evaluate differences between more than two data sets.

2.1. Production, purification, conjugation and characterization of ADAPT molecules

Production and Purification. The genes encoding ADAPT6-SSSG-ADAPT6, ADAPT6-$(SSSG)_2$-ADAPT6, ADAPT6-$(SSSG)_3$-ADAPT6 were synthesized by Thermo Fisher Scientific (Waltham, MA USA) and PCR amplified using primers introducing the amino acid sequences MGVDANS and GSSC in the N- and C-terminus, respectively. A monomeric version of ADAPT6 with the N-terminal sequence MG-$(HE)_3$-DANS and the C-terminal sequence GSSC was generated as a control, as described earlier [18]. The amplified sequences were subcloned into a T7 inducible expression vector and the sequences were verified using DNA-sequencing by Microsynth AG (Balgach, Switzerland). The ADAPT6 variants were produced in *E. coli* BL21* (DE3) cells and protein lysates were collected as previously described [7]. The lysates were heat-treated for 10 min in 90 °C and precipitated endogenous *E. coli* proteins were removed by centrifugation. The lysates containing the dimeric ADAPT6 variants were incubated with 30 U/ml Benzonase® endonukleas (Merck, Darmstadt, Germany) at 37 °C, 150 rpm for 18 h followed by centrifugation. The buffer of the lysates was changed to 20 mM Tris, pH 8.0, using Vivaspin concentrators (MWCO 5000 Da, Merck, Darmstadt, Germany). The thiol group of the terminal cysteine was reduced by incubation with 5 mM dithiothreitol (DTT) at 37 °C for 40 min to avoid dimerization of the proteins. The lysates were loaded onto an anion exchange column (Resource Q, GE Healthcare, Uppsala, Sweden) and eluted using a 0–0.5 M NaCl gradient. The monomeric control construct was purified using immobilized metal affinity chromatography (IMAC) with a Ni^{2+}-resin.

Proteins intended for radioiodination were further purified using a semipreparative reversed phase high performance liquid chromatography (RP-HPLC) column (Zorbax, 300SB-C18, 9.4 × 250 mm, 5 μm particle size, Agilent). Dimeric proteins were eluted using a gradient of 60–80% B (A, 0.1% trifluoroacetic acid in water; B, 0.1% trifluoroacetic acid in acetonitrile) over 20 min using a flow rate of 3 mL/min. The monomeric protein was eluted using a gradient of 33–38% B over 25 min at the same flow rate. The purity and molecular weights of the proteins were analysed using sodium dodecyl sulfate polyacrylamide gel electrophoreses (SDS-PAGE) and liquid chromatography-electrospray ionization-mass spectrometry (LC-ESI-MS) using a 6520 Accurate Q-TOF LC/MC (Agilent, CA, USA).

Conjugation of DOTA. ADAPT6 variants, intended for metal-labelling, were conjugated with a maleimido derivate of the DOTA chelator

maleimido-monoamide-DOTA (Macrocyclics, TX, USA) through the thiol group of the cysteines. The thiol groups were reduced by incubation with 20 mM DTT for 30 min at 40 °C prior conjugation. Excess of DTT was removed using PD-10 size-exclusion columns, and proteins were eluted in 20 mM NH_4Ac, pH 5.5. A 2-fold molar excess of maleimido-DOTA was added to each protein followed by incubation at 55 °C for 2 h. Excess DOTA and unconjugated proteins were removed using RP-HPLC as described above. The purified proteins were alkylated with indoacetoamide (IAA) (Merck, Darmstadt, Germany) to ensure blocking of remaining reactive thiol groups. Excess of IAA was removed using PD-10 size exclusion columns. The purity of the non-conjugated and DOTA-conjugated ADAPT6 variants were evaluated using SDS-PAGE and RP-HPLC with an analytical column (Zorbax 300 SB-C18 4.6 × 150 mm, 3.5 μm particle size) using a gradient of 35–85% B over 30 min (A, 0.1% trifluoroacetic acid in water; B, 0.1% trifluoroacetic acid in acetonitrile) with a flow rate of 1.2 mL/min. The proteins were lyophilized in 50 μg aliquots.

Characterization of ADAPT6 dimers. The secondary structure and thermal stability were determined for the three dimeric variants using a Chirascan™ circular dichroism spectrometer (Applied Photophysics, Surrey, UK). The proteins were diluted to 0.4 mg/mL in PBS and the secondary structure and the refolding capacity of the different variants were assessed by measuring the degree of ellipticity from 195 to 250 nm at 25 °C before and after heat-treatment. The melting temperatures were determined by measuring the change in ellipticity at 221 nm during a temperature gradient ranging from 25 to 90 °C.

The affinity to HER2 was determined using a Biacore T200 instrument (Biacore Life Science, GE Healthcare, Uppsala, Sweden). Recombinant human HER2 (Sino Biological, Beijing, China) was immobilized on one flow-cell surfaces of a CM5 sensor chip to a response level of 1100 RU by amine coupling. A 1:2 dilution series with five concentrations starting from 50 nM was prepared in PBS supplemented with 0.05% Tween (PBST), pH 7.4, for each variant. The variants were injected with a flow rate of 30 μL/min for 300 s followed by 1600 s of dissociation. The regeneration was carried out by injecting 15 μL of 10 mM HCl. The dissociation equilibrium (K_D), the association rate (k_a), and the dissociation rate (k_d) constants were calculated using the Biacore T200 Evaluation Software 2.0, assuming a 1:1 interaction model.

2.2. Labelling

Radiolabeling was evaluated only for DiADAPT6L2 and DiADAPT6L3 since SPR experiments demonstrated that DiADAPT6L1 had appreciable lower affinity to HER2.

Labelling of DOTA-DiADAPT6L2 and DOTA-DiADAPT6L3 with ^{111}In. Lyophilized ADAPT6 variants (15 μg) were reconstituted in 0.2 M ammonium acetate, pH 5.5, and incubated with 110 μL of ^{111}In solution (30–35 MBq in 0.05 M hydrochloric acid) at 95 °C for 60 min followed by challenging with 500-fold molar excess EDTA at 95 °C for 20 min. The radiolabelled ADAPT6 variants were purified from unbound ^{111}In using disposable NAP-5 size-exclusion columns (GE Healthcare, Uppsala, Sweden). Radiochemical yield and purity of conjugates were determined using radio-ITLC. Authenticity of conjugates was confirmed using radio-SDS PAGE.

To evaluate the stability of the labelling, the radiolabelled conjugates were incubated with a 500-fold molar excess of EDTA at room temperature for 2 h, and the percentage of protein-based radioactivity was determined using radio-ITLC.

Indirect radioiodination of DiADAPT6L2 and DiADAPT6L3 using ^{125}I. Radioiodination was performed according to methods developed earlier for affibody molecules [38] (Fig. 2). Before radioiodination, the spontaneously formed intermolecular disulfide bridges were reduced by incubation with 15 M dithiothreitol (DTT) for 60 min at 37 °C. The mixture was applied to NAP-5 size-exclusion columns, pre-equilibrated and eluted with well-degassed 0.2 M acetate buffer, pH 6.0. For radioiodination of HPEM, 7.5 μL ^{125}I-iodide stock solution (25 MBq) was mixed with 5 μL of a 5% solution of acetic acid in methanol and 5 μL of a solution of HPEM (1 mg/ml in 5% acetic acid in methanol). 40 μg chloramine-T in 5 μL water was added and the mixture was incubated for 5 min at ambient temperature. The reaction was quenched by adding 60 μg sodium metabisulfite in 5 μL water. Immediately after labelling of HPEM, a solution of DiADAPT6L variants in 0.2 M acetate buffer was added and the mixture was incubated at room temperature for 60 min. The yield was determined by ITLC eluted with acetone:-water (7:3). The radiolabelled conjugates were purified using a NAP-5 column pre-equilibrated with PBS. The radiochemical purity of the conjugates was assessed using ITLC eluted with 70% acetone.

2.3. In vitro evaluation

In vitro *specificity*. Specificity of binding of radiolabelled ADAPT6 derivatives to HER2-expressing cancer cells was tested using ovarian carcinoma SKOV-3 (1.6×10^6 receptors/cell) and breast carcinoma BT-474 (2×10^6 receptors/cell) cell lines according to methods described earlier [40].

To test the binding specificity, 5 nM of the labelled variants was added to six petri dishes (ca. 10^6 SKOV-3 or BT-474 cells/dish). To saturate the receptors, a 100-fold molar excess of non-labelled DiADAPT6 molecules was added to three petri dishes 15 min before adding the labelled conjugates. The dishes were incubated at 37 °C for 1 h in a humidified incubator. The media was collected, the cells were detached using trypsin-EDTA solution and radioactivity was measured. Percent of cell-bound radioactivity was calculated for both the pre-saturated and unsaturated cells.

Affinity determination using LigandTracer. SKOV-3 human ovarian carcinoma cells were seeded on a local area of a cell culture dish (NunclonTM, Size 100620, NUNC A/S, Roskilde, Denmark), as described previously [41]. The binding of ADAPT6 molecules labelled with ^{111}In and ^{125}I to living cells was monitored in real-time at room temperature using LigandTracer yellow and grey (Ridgeview instruments AB, Uppsala, Sweden), using established methods [41]. Cells were incubated with two increasing concentrations of the radioconjugate (0.3 and 1 nM) followed by monitoring dissociation while cells were incubated with fresh medium. Analysis was performed in duplicates. Interaction curves were analysed to determine the affinity and rate constants using TraceDrawer evaluation software.

Cellular processing. The rate of internalization of radiolabelled ADAPT6 dimers by SKOV-3 and BT-474 cells during continuous incubation was studied using the acid wash method [40]. The labelled compounds (protein concentration of 5 nM) were added to 15 petri dishes containing approximately 10^6 cells/dish. The cells were incubated at 37 °C in a humidified incubator. At five time points (1, 2, 4, 8 and 24 h after incubation start), the medium from a set of three dishes was removed and the cells were washed with 1 mL of ice-cold serum free medium. The cells were treated with 0.2 M glycine buffer containing 4 M urea, pH 2.0, for 5 min on ice in order to collect the membrane-bound radioactivity. To collect the internalized radioactivity, the cells were treated with 0.5 mL of 1 M NaOH at 37 °C for 30 min.

2.4. Animal studies

Animal studies were planned and performed in agreement with EU Directive 2010/63/EU for animal experiments and Swedish national legislation concerning protection of laboratory animals. Experiments were approved by the Ethics Committee for Animal Research in Uppsala.

Tumour-targeting properties of ^{111}In and ^{125}I-labelled ADAPT6 variants were evaluated in BALB/C nu/nu mice bearing SKOV-3 xenografts with high HER2 expression. Information concerning molecular weights of the evaluated constructs is presented in Table 3. Mice

bearing A431 xenografts with very low HER2 expression were used as negative controls. Xenografts were established by subcutaneous implantation of 10^7 SKOV-3 or A431 cells. At the time of the experiments, the average animal weight was 18 ± 1 g. The average tumour weights were 0.17 ± 0.07 g and 0.23 ± 0.7 g, for SKOV-3 and A431 xenografts, respectively. A group of four mice was used for each data point. A dual-label approach was used in biodistribution studies to reduce the number of tumour-bearing mice. For each ADAPT6 construct, ^{125}I-labeled (15 kBq per mouse) and ^{111}In-labeled proteins (15 kBq per mouse) were mixed and the total protein dose was adjusted to 0.8 nmol/mouse using the corresponding non-labelled protein. The injected volume was adjusted with PBS to 100 μL/mouse. The animals were injected in the tail veins. The biodistribution in mice bearing SKOV-3 xenografts was measured at 1 and 4 h post injection (p.i.). The biodistribution in the control group with A431 xenografts was measured at 4 h p.i. Euthanasia was performed using a lethal dose of Rompun/Ketalar anaesthesia. Animals were exsanguinated and dissected. The tissue samples were weighed, and their radioactivity was measured using an automated γ-spectrometer. The ^{125}I radioactivity was measured in the energy window from 5 to 90 keV and ^{111}In from 115 to 600 keV. The data were corrected for dead time, spillover, and background. The tissue uptake values were calculated as percent of injected dose per gram tissue (%ID/g).

To confirm that dimeric constructs could visualize HER2-expressing tumours, whole body SPECT/CT scans of the mice injected with ^{111}In-labeled DOTA-DiADAPT6L3 over DOTA-DiADAPT6L2 (0.8 nmol, 2.5 μg MBq) were performed using nanoScan SC (Mediso Medical Imaging Systems, Hungary) at 4 h and 24 h p.i. as describe earlier [18].

3. Results

3.1. Production, purification, conjugation and characterization of ADAPT dimers

Three ADAPT6 dimers with different linkers ((S_3G), $(S_3G)_2$, or $(S_3G)_3$) were produced in *E. coli* and purified using heat-treatment followed by anion-exchange chromatography. The constructs were denoted DiADAPT6L1, DiADAPT6L2 and DiADAPT6L3. The monomer $(HE)_3$-DANS-ADAPT6-GSSC was produced and purified for comparison. Proteins intended for ^{111}In labelling were conjugated with maleimide-DOTA and excess of DOTA and unconjugated ADAPT6 dimers were removed by RP-HPLC. The thiol group of any remaining unconjugated proteins was successfully blocked with IAA. The purity of all constructs was above 95%, determined by analytical RP-HPLC and mass spectrometry confirmed correct molecular masses.

The circular dichrosim analysis showed similar spectra for two of the constructs, with two local inflection points at 208 and 221 nm, indicating high alpha helical content (Fig. 3). However, the construct with the shortest linker, DiADAPT6L1, was shown to have very low alpha helicity, indicating that the protein is not able to fold properly. This dysfunctionality of the protein can also be seen when assessing the affinity to HER2 (Table 1). The melting temperatures for the constructs were determined to 62 °C and 64 °C for DiADAPT6L2 and DiADAPT6L3, respectively. Due to the low structural content of DiADAPT6L1, melting temperature could not be assessed for DiADAPT6L1. However, all three dimeric constructs showed spectra that overlapped well after thermal denaturation (Fig. 3).

Table 1
Kinetic parameters for the dimeric ADAPT6 variants interacting with HER2, measured using surface plasmon resonance.

	k_a (Ms^{-1})	k_d (s^{-1})	K_D (M)
DOTA-DiADAPT6L1	1×10^4	1.8×10^{-4}	1.8×10^{-8}
DOTA-DiADAPT6L2	8.9×10^4	2.3×10^{-5}	2.5×10^{-10}
DOTA-DiADAPT6L3	1.3×10^5	2.7×10^{-5}	2.1×10^{-10}

HER2-binding analysis by SPR (Fig. 4) showed K_D values in the subnanomolar range for DOTA-DiADAPT6L2 and DOTA-DiADAPT6L3, 0.25 nM and 0.2 nM respectively. For DOTA-DiADAPT6L1 the affinity was approximately 100-times lower (Table 1). Monomeric versions of ADAPT6 have previously demonstrated affinities around 2.5 nM using SPR [8]. Thus, the 10-times higher apparent affinities of DOTA-DiADAPT6L2 and DOTA-DiADAPT6L3 compared to the monomeric constructs implies that the interaction to HER2 benefits from an avidity affect. The lower affinity of DOTA-DiADAPT6L1 indicates that the HER2-binding interface of the ADAPT6 units is either not correctly folded or not as accessible as in the other two dimeric constructs. DOTA-DiADAPT6L1 was excluded from further studies due to the less favourable characteristics compared to the other two variants.

3.2. Radiolabelling

DOTA-DiADAPT6L2 and DOTA-DiADAPT6L3 were labelled with ^{111}In to radiochemical yields of 72 and 62%, respectively. The radiochemical purity after size-exclusion chromatography was over 99% for both conjugates. A challenge with 500-fold excess of EDTA during 2 h did not reveal any release of radionuclides from the conjugates.

The site-specific indirect radioiodination of ADAPT6 dimers using HPEM was in a good agreement with earlier published results for radioiodination of ADAPT6 monomers [17]. The radioiodination yield of HPEM was 97%. The overall yield of radioiodination of DiADAPT6L2 and DiADAPT6L3 using HPEM was 65–67%.

3.3. In vitro binding specificity and affinity

The binding of the radiolabelled ADAPT6 dimers to both HER2-expressing SKOV-3 and BT-474 cells was significantly ($p < 0.0005$) reduced after pre-saturation of the receptors by non-labelled ADAPT6 dimers. This demonstrated that the binding was saturable and confirmed its HER2-specific character (Fig. 5).

Representative sensorgrams of binding of the ADAPT6 dimer ^{111}In-DOTA-DiADAPT6L2 and the parental monomer ^{111}In-DOTA-VDANS-ADAPT6 to living HER2-expression SKOV-3 cells are presented in Fig. 6. The sensorgram of ^{111}In-DOTA-DiADAPT6L2 reflects the essential

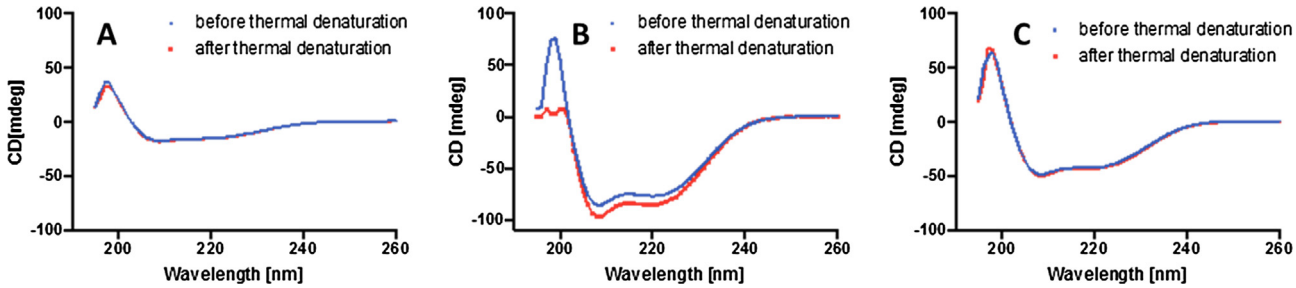

Fig. 3. CD measurements of secondary structure before and after variable temperature measurements of DOTA-DiADAPT6L1 (A), DOTA-DiADAPT6L2 (B), and DOTA-DiADAPT6L3 (C).

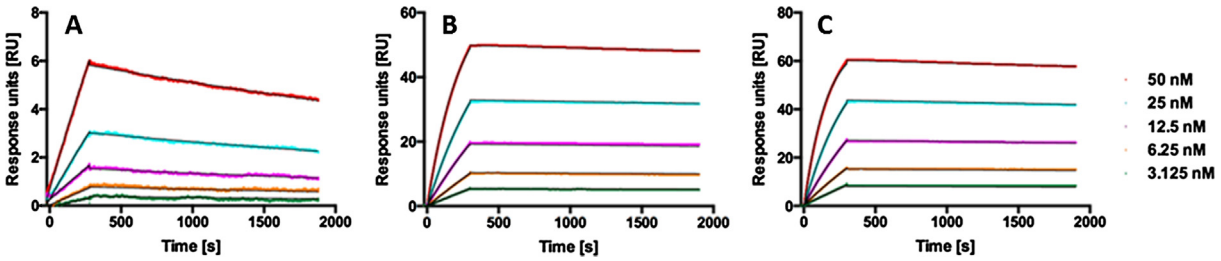

Fig. 4. Biosensor binding analysis using surface plasmon resonance. Sensorgrams obtained after injection of DOTA-DiADAPT6L1 (A), DOTA-DiADAPT6L2 (B), and DOTA-DiADAPT6L3 (C) onto a chip immobilized with HER2.

feature of the interaction of dimeric ADAPT6 variants with HER2-expressing cells; very slow dissociation (Fig. 6A) compared to the monomer (Fig. 6B).

According to LigandTracer measurements, the binding of all dimeric ADAPT6 variants to living cells was best fitted to a 1:1 interaction model according to Langmuir, indicating that the interaction was dominated by one type of interactions with HER2. Dissociation equilibrium constant (K_D) values for the interaction between ADAPT dimers and HER2-expressing SKOV-3 cells are presented in Table 2. All variant demonstrated affinity in low picomolar range.

Data concerning cellular processing and internalization of ^{111}In-DOTA-DiADAPT6L2 and ^{111}In-DOTA- DiADAPT6L3 are presented in Fig. 7. The rapid binding during the first hour was followed by a slower increase of cell-associated radioactivity. There was a cell-line specific difference in the binding pattern. The increase of the binding in the second phase was much more pronounced for the BT-474 cell line. Internalization of the conjugates was relatively slow, below 30% after 24 h, for both types of conjugates in both cell lines.

The cellular processing pattern was clearly different for ADAPTs labelled with the non-residualizing ^{125}I-HPEM label (Fig. 8). In SKOV-3 cells, the maximum cell-bound radioactivity was observed around 4 h after the incubation started (Fig. 8A and C). Thereafter, the cell-bound radioactivity decreased slowly. The internalized fraction did not increase continuously, as in the case when using the residualizing radiometal label but reached a plateau at 4 h (on the level of approximately 10% maximum cell-bound radioactivity). The pattern was somewhat different in BT-474 cells (Fig. 8B and D). Some increase of cell-associated radioactivity was observed after 4 h, but this increase was appreciably smaller than in the case of the residualizing ^{111}In-DOTA label. There was also some minor increase of internalized radioactivity after 4 h. Overall, the linker size had much smaller (if any) effect on the pattern of cellular processing than the nature of the label and the processing of HER2 of the particular cell line.

3.4. Animal studies

To test if the accumulation of radiolabelled dimeric ADAPT6 constructs in tumours is HER2-dependent, uptake in SKOV-3 xenografts with high HER2 expression and A431 xenografts with low HER2 expression was measured (Fig. 9). The uptake of all four tested dimers in SKOV-3 was significantly ($P < 0.001$) higher than in A431 xenografts, which indicates HER2-dependent accumulation.

The data concerning comparison of biodistribution of monomeric and dimeric forms of ADAPT6 are presented in Table 4. Most of the biodistribution characteristics of the dimeric variants of ADAPT6 followed the pattern of the monomeric ADAPT6. All variants underwent renal clearance from blood but with high reabsorption in proximal tubuli of the kidneys. This resulted in rapid decrease of blood-born radioactivity to less than 0.5 %ID/g at 4 h p.i. for all variants, and low accumulation in the majority of the normal tissues. The difference between using residualizing ^{111}In or non-residualizing ^{125}I labels also showed a similar pattern regarding kidney uptake for the dimeric variants of ADAPT6 as for the monomeric version; iodine-labelled ADAPT6 constructs cleared rapidly from kidneys, while the renal retention of ^{111}In-labelled constructs was high.

However, there were apparent differences in biodistribution pattern between the dimeric and the monomeric formats of ADAPT6 in several of the other organs. In the case of ^{111}In labelled ADAPT6 variants, both dimeric forms had significantly ($p < 0.05$) higher uptake in liver, spleen and stomach at 4 h after injection, and higher uptake in blood,

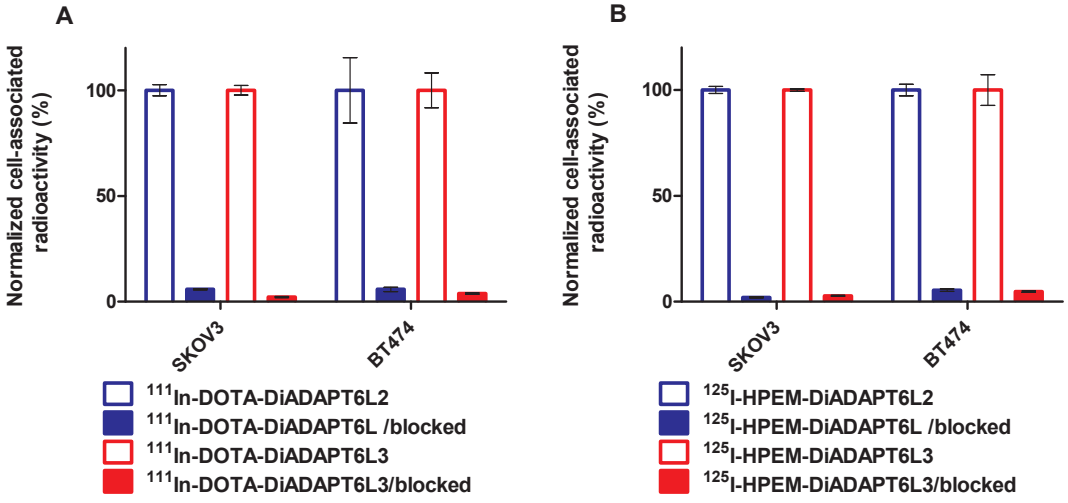

Fig. 5. Binding specificity of ^{111}In-DOTA-DiADAPT6L2 and ^{111}In-DOTA-DiADAPT6L3 (A), and ^{125}I-HPEM-DiADAPT6L2 and ^{125}I-HPEM- DiADAPT6L3 (B) to HER2 expressing SKOV-3 and BT-474 cells. For receptor blocking, a 100-fold molar excess of the corresponding nonlabelled DiADAPT6 was added. Data are presented as mean values with standard deviations (n = 3).

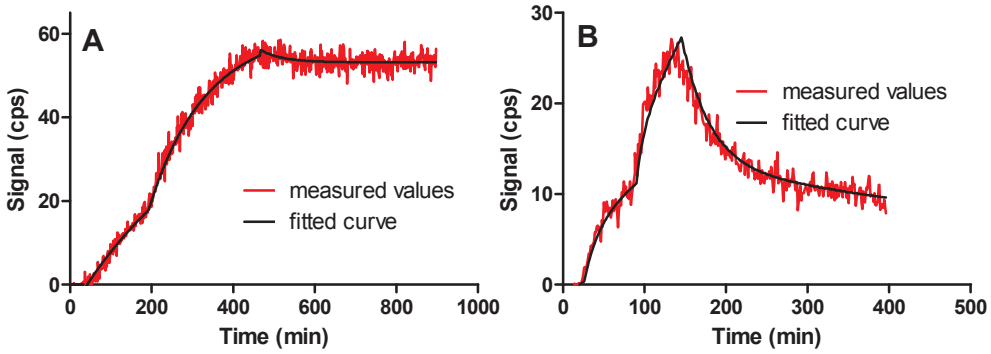

Fig. 6. Representative sensorgram of binding of radiolabeled ADAPT6 dimer ^{111}In-DOTA-DiADAPT6L (A) and the parental monomer ^{111}In-DOTA-VDANS-ADAPT6 (B) to HER2-expressing SKOV-3 cells.

Table 2
Dissociation equilibrium constants (K_D) for the interaction of radiolabelled dimeric ADAPT6 variants with HER2-expressing SKOV-3 cells, determined using the TraceDrawer software.

	K_D (pM)	
	DiADAPT6L2	DiADAPT6L3
^{111}In-DOTA	35 ± 7	150 ± 70
^{125}I-HPEM	260	115 ± 15

Table 3
Molecular weights of ADAPT6 variants evaluated in the biodistribution study.

	Molecular weight (kDa)	
	^{125}I-HPEM label	^{111}In-DOTA label
DiADAPT6L2	12.039	12.332
DiADAPT6L3	12.358	12.650
ADAPT6 monomer	7.021	7.314

liver and spleen at 24 h p.i. than the monomeric counterpart. The differences were not as pronounced when using the radioiodine label. The length of the linker had no significant impact on biodistribution of the dimeric variants.

The most striking was the difference in tumour uptake. The uptake of the dimeric forms was significantly ($p < 0.05$) lower than the uptake of the monomeric variant at both time points when using both residualizing and non-residualizing labels.

The tumour-to-organ ratios also reflect the differences in biodistribution and targeting pattern between the dimeric ADAPT6 and the monomeric variant (Table 5). The difference in tumour-to-organ ratios between ^{125}I-HPEM-ADAPT6 and ^{125}I-HPEM- DiADAPT6L3 was not statistically significant at 4 p.i., but there was a tendency that the monomeric form provided higher average values. At all other data points, the monomeric form provided significantly higher tumour-to-organ ratios.

The microSPECT/CT imaging experiment confirmed the results of the biodistribution study (Fig. 10). HER2-expressing SKOV-3 xenografts were clearly visualized using both ^{111}In-DOTA-DiADAPT6L2 and ^{111}In-DOTA-DiADAPT6L3 at both 4 and 24 h p.i.. The radionuclide accumulation in kidneys was appreciably higher than the accumulation in tumours. The radioactivity concentration of the content of urinary bladder at 4 h p.i. was also higher than the tumour uptake. The uptake in all other organs and tissue was substantially lower than in tumours. This provided high contrast imaging of HER2 expression.

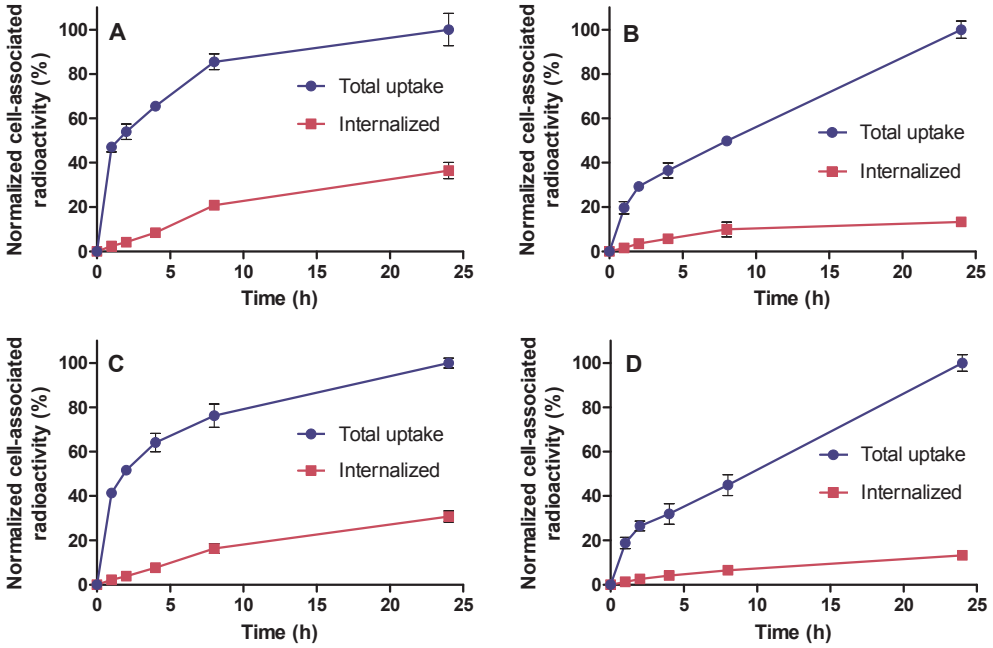

Fig. 7. Binding and cellular processing of ^{111}In-DOTA-DiADAPT6L2 (A, B) and ^{111}In-DOTA-DiADAPT6L3 (C, D) during continuous incubation with HER2-expressing SKOV-3 (A, C) and BT-474 (B, D) cells. Values are normalized to the maximum cell-bound activity. Data are presented as mean values with standard deviations from three cell dishes.

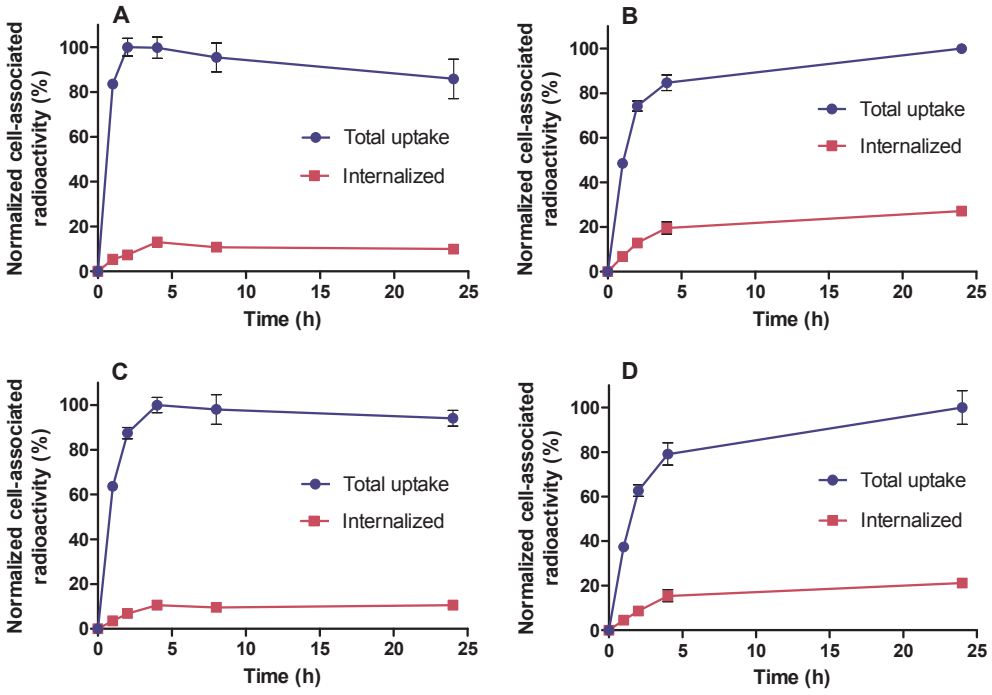

Fig. 8. Binding and cellular processing of ^{125}I-HPEM-DiADAPT6L2 (A, B) and ^{125}I-HPEM-DOTA-DiADAPT6L3 (C, D) during continuous incubation with HER2-expressing SKOV-3 (A, C) and BT-474 (B, D) cells. Values are normalized to the maximum cell-bound activity. Data are presented as mean values with standard deviations from three cell dishes.

4. Discussion

Mathematic modelling suggests that small (less than 25 kDa) targeting proteins offer an advantage in tumour targeting due to better extravasation and quicker diffusion inside tumours [42]. However, this requires high affinity of the targeting protein to its tumour-associated molecular target [42]. Dimerization is a possible way to improve the apparent affinity of the interaction. A bivalent binding reduces the probability of dissociation of the whole targeting moiety if one of the paratope dissociates. In addition, the probability of rebinding after dissociation is higher for a dimeric construct compared to a monomer.

Still, one has to take into account the potential issue of mutual steric hindrance of the binding by the two fused monomeric units. In this study, the use of the short linker S_4G between the two ADAPTs resulted in an appreciable loss of binding strength. This is in agreement with the observation of Krasniqi and co-authors [34] who have found that the use of a short G_4S linker for dimerization of sdAbs resulted in decrease of an apparent affinity. At the same time, the use of longer linkers increased the affinity from 1.2 nM for the parental monomeric format [15] to approximately 0.25 nM (according to SPR measurements) for the dimeric formats, i.e. more than five-fold. There was essentially no difference in binding affinity of DiADAPT6L2 and DiADAPT6L3, which indicates that additional increase of the linker length would not offer further enhancement in affinity.

Another essential aspect of the molecular design of ADAPT derivatives for radionuclide targeting is the preserved refolding capacity. Both original ABD and ADAPT6 denature when exposed to an elevated temperature, non-physiological pH or lipophilic solvents, but refold as soon as returned back to physiological temperatures and chemical environment [4,8]. Such feature enables the use a broad spectrum of methods for radiolabelling or conjugation of other payloads. For example, the use of macrocyclic chelators provides high kinetic inertness of the radiometal-chelator complex, which excludes dissociation of the radionuclide from the targeting conjugate in vivo [43]. However, a downside of this high inertness is the necessity to perform the labelling at elevated temperature, up to 95 °C [43]. Taking this into account, the preserved refolding ability (Fig. 3) is an advantage of ADAPT6.

Both DiADAPT6L2 and DiADAPT6L3 were labelled with good yield and excellent stability with the residualizing radiometal ^{111}In using a DOTA chelator and with the non-residualizing radiohalogen ^{125}I using a HPEM linker. Both approaches utilized maleimido-containing prosthetic groups for coupling. Importantly, the ADAPT scaffold does not contain cysteines. Introduction of a single cysteine in a desired position creates a unique thiol group in the whole protein. Application of a thiol-directed chemistry permits therefore a site-specific labelling, resulting in well-define conjugates with reproducible biochemical and pharmacological properties. This is a clear advantage of our labelling approach compared to the commonly used amine-directed chemistry. Each

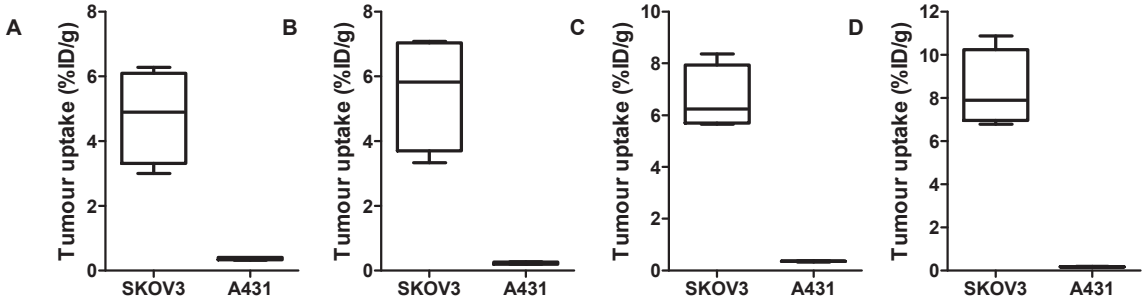

Fig. 9. Specificity of HER2 targeting in vivo. Uptake of ^{111}In-DOTA-DiADAPT6L2 (A), and ^{125}I-HPEM-DiADAPT6L2 (B), ^{111}In-DOTA-DiADAPT6L3 (C), and ^{125}I-HPEM- DiADAPT6L3 (D) in SKOV-3 (high HER2 expression) and A431 (very low HER2 expression) xenografts at 4 h p.i. Data are presented as mean values with standard deviations (n = 4).

Table 4
Biodistribution of radiolabelled ADAPT6 variants in BALB/C nu/nu mice bearing SKOV-3 xenografts.

	^{125}I-HPEM- ADAPT6	^{111}In-DOTA-ADAPT6	^{125}I-HPEM- DiADAPT6L2	^{111}In-DOTA-DiADAPT6L2	^{125}I-HPEM- DiADAPT6L3	^{111}In-DOTA-DiADAPT6L3
4 h						
Blood	0.26 ± 0.03[a]	0.08 ± 0.01	0.23 ± 0.05[a]	0.13 ± 0.02	0.24 ± 0.07[a]	0.13 ± 0.01[b]
Lung	0.20 ± 0.02	0.11 ± 0.03	0.19 ± 0.01	0.3 ± 0.1	0.3 ± 0.2	0.26 ± 0.02[b]
Liver	0.9 ± 0.3[a]	0.22 ± 0.01	0.6 ± 0.3	0.55 ± 0.08[b]	0.6 ± 0.2	0.49 ± 0.06[b]
Spleen	0.2 ± 0.1	0.10 ± 0.03	0.15 ± 0.04	0.24 ± 0.04[b]	0.17 ± 0.05	0.24 ± 0.04[b]
Stomach	1.2 ± 0.5[a]	0.09 ± 0.01	0.7 ± 0.3[a]	0.21 ± 0.06[b]	1.0 ± 0.3[a]	0.19 ± 0.03[b]
Kidney	0.83 ± 0.05[a]	316 ± 19	1.3 ± 0.4[a,b]	315 ± 25	1.1 ± 0.2[a]	327 ± 24
Tumour	13 ± 3[a]	12 ± 3	6 ± 2[a,b]	5 ± 1[b]	8 ± 2[a]	7 ± 1
Muscle	0.12 ± 0.04	0.05 ± 0.02	0.09 ± 0.03[b]	0.11 ± 0.02[b]	0.08 ± 0.05	0.08 ± 0.01
Bone	0.21 ± 0.05[a]	0.10 ± 0.04	0.10 ± 0.03[a,b]	0.27 ± 0.07[b]	0.1 ± 0.1	0.14 ± 0.05[b]
24 h						
Blood	0.027 ± 0.004[a]	0.022 ± 0.001	0.022 ± 0.002[a]	0.04 ± 0.01[b]	0.021 ± 0.003[a]	0.035 ± 0.004[b]
Lung	0.02 ± 0.01	0.06 ± 0.05	0.017 ± 0.004	0.1 ± 0.1	0.02 ± 0.01[a]	0.11 ± 0.02
Liver	0.09 ± 0.01[a]	0.14 ± 0.01	0.06 ± 0.01[a,b]	0.31 ± 0.04[b]	0.057 ± 0.003[a,b]	0.28 ± 0.03[b]
Spleen	0.03 ± 0.02[a]	0.09 ± 0.03	0.03 ± 0.02[a]	0.18 ± 0.05[b]	0.02 ± 0.01[a]	0.19 ± 0.03[b]
Stomach	0.03 ± 0.01	0.06 ± 0.04	0.03 ± 0.02	0.10 ± 0.02	0.027 ± 0.005[a]	0.08 ± 0.04
Kidney	0.18 ± 0.02[a]	298 ± 43	0.3 ± 0.1[a]	236 ± 8[b]	0.24 ± 0.03[a]	277 ± 43
Tumour	6 ± 2[a]	9 ± 3	1.2 ± 0.4[a,b]	3.2 ± 0.6[b]	1.6 ± 0.3[a,b]	3.6 ± 0.4[b]
Muscle	0.009 ± 0.004	0.05 ± 0.03	0.005 ± 0.003	0.09 ± 0.06	0.003 ± 0.002[b]	0.042 ± 0.007
Bone	0.07 ± 0.04	0.11 ± 0.07	0.02 ± 0.01	0.2 ± 0.2	0.02 ± 0.01	0.09 ± 0.02

Results are presented as an average %ID/g with standard deviation of 4 animals.
[a] Significant difference ($p < 0.05$) between ^{111}In- and ^{125}I-labelled variants of the same construct;
[b] Significant difference ($p < 0.05$) between this dimer and the monomer labelled with the same nuclide;

ADAPT6 monomer contains four lysines and the N-terminal amino group. Coupling of labels using an amine-directed method (using of e.g. succinimidyl- or isothiocyanato derivatives) would result in a random distribution of these labels along the solvent-exposed surface of the protein. Accordingly, the product would contain a mixture of protein domains with different properties of the surface (distribution of charge) and therefore different binding and biodistribution properties. Our directed labelling approach circumvents this.

The results of LigandTracer measurement of binding of radiolabelled ADAPT6 dimers to living HER2-expressing cells (Fig. 6 and Table 2) were in agreement with the SPR measurements. The dimers showed a clear reduction of the dissociation rate compared with the parental monomeric form (Fig. 6). An interesting finding is that the interaction of the dimers with HER2 on living cells was best fitted to the 1:1 interaction model suggesting that binding is strongly dominated by one type of interaction. The 1 to 1 interaction according to Langmuir model means that a ligand binds to a target with a monovalent stoichiometry and that the target population presents a single binding site with uniform strength of binding, as opposed e.g. bivalent binding or presence of target molecules in different conformations resulting in presence of two binding sites with different affinities. Most likely the total length of the construct is insufficient to engage two HER2 receptors simultaneously.

The internalization rate is essential for selection of an optimal labelling strategy [44]. Internalization of a target-ligand complex, results in trafficking to the lysosomal compartment and thereafter proteolytic degradation. Depending of the physicochemical properties of the radiometabolites, the fate of the intracellular radioactivity will be different. If the catabolites are lipophilic, they can penetrate both lysosomal and cellular membranes and thereby leave the cells. This is often the case when using radiohalogens for labelling. Such kind of labels is termed non-residualizing labels. Radiometal-chelator complexes are

Table 5
Tumour-to-organ ratios of radiolabelled ADAPT6 variants in BALB/C nu/nu mice bearing SKOV-3 xenografts.

	^{125}I-HPEM- ADAPT6	^{111}In-DOTA-ADAPT6	^{125}I-HPEM- DiADAPT6L2	^{111}In-DOTA-DiADAPT6L2	^{125}I-HPEM- DiADAPT6L3	^{111}In-DOTA-DiADAPT6L3
4 h						
Blood	54 ± 17[a]	149 ± 21	24 ± 7[b]	37 ± 13[b]	37 ± 10[a]	50 ± 8[b]
Lung	67 ± 26[a]	103 ± 24	29 ± 10[b]	18 ± 4[b]	31 ± 16	24 ± 4[b]
Liver	15 ± 3[a]	53 ± 13	10 ± 6	9 ± 2[b]	15 ± 3	14 ± 1[b]
Spleen	76 ± 43[a]	121 ± 45	41 ± 16[a]	20 ± 8[b]	53 ± 20	28 ± 3[b]
Stomach	14 ± 8[a]	136 ± 29	9 ± 5[a]	24 ± 9[b]	9 ± 3[a]	35 ± 6[b]
Kidney	16 ± 4[a]	0.037 ± 0.008	5 ± 2[a,b]	0.037 ± 0.008	8 ± 2	0.021 ± 0.002[b]
Muscle	129 ± 66	263 ± 179	68 ± 34	43 ± 12[b]	127 ± 62	86 ± 14[b]
Bone	67 ± 25[a]	133 ± 31	62 ± 34	18 ± 5[b]	85 ± 43	53 ± 25[b]
24 h						
Blood	228 ± 65[a]	431 ± 143	52 ± 14[b]	81 ± 25[b]	77 ± 12[a,b]	103 ± 9[b]
Lung	293 ± 127	154 ± 88	75 ± 30[b]	28 ± 11[b]	167 ± 101[a,b]	33 ± 4[b]
Liver	66 ± 27	68 ± 25	19 ± 5	10 ± 1[b]	29 ± 4[a,b]	13 ± 1[b]
Spleen	161 ± 101	106 ± 28	40 ± 12[b]	19 ± 2[b]	97 ± 60	20 ± 3[b]
Stomach	192 ± 28	181 ± 82	49 ± 14[b]	33 ± 8[b]	64 ± 24	51 ± 29[b]
Kidney	36 ± 15[a]	0.03 ± 0.01	4 ± 1[a,b]	0.014 ± 0.003[b]	7 ± 1[a,b]	0.013 ± 0.001[b]
Muscle	779 ± 372[a]	222 ± 63	266 ± 104[a,b]	50 ± 27[b]	409 ± 123	87 ± 21[b]
Bone	119 ± 59	116 ± 61	65 ± 38	26 ± 23	93 ± 4[a]	42 ± 8

Results are presented as an average %ID/g with standard deviation of 4 animals.
[a] Significant difference ($p < 0.05$) between ^{111}In- and ^{125}I-labelled variants of the same construct.
[b] Significant difference ($p < 0.05$) between this dimer and the monomer labelled with the same nuclide.

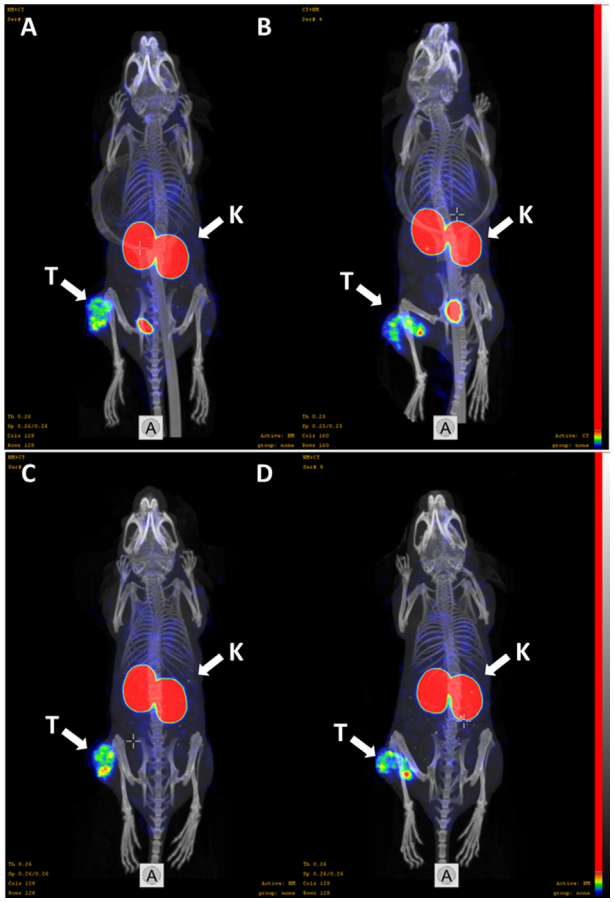

Fig. 10. MicroSPECT/CT imaging (maximum intensity projections) of HER2-expressing SKOV-3xenografts using ADAPT6 molecules at 4 h p.i. (A and B) and 24 h pi (C and D). Imaging using ^{111}In-DOTA-DiADAPT6L2 (A and C) and ^{111}In-DOTA-DiADAPT6L3 (B and D). The linear colour scale was adjusted to provide clear visualization of the tumours. Arrows point at tumours (T) and kidneys (K).

often charged and nearly always hydrophilic. Such radiometabolites cannot penetrate the cellular membrane and therefore they accumulate inside the cell. Such labels are termed as residualizing [44]. The use of residualizing labels increases the accumulation of radioactivity in tumours, but also increases retention of the radionuclide in normal tissues if it is internalized. This is often the case with excretory organs. In the case of slow internalization by cancer cells, a non-residualizing label might be preferable since the loss of activity from tumours might be minor, but clearance from excretory organs would be rapid. This is particularly important for ADAPTs, which are readily reabsorbed in proximal tubuli of kidneys after glomerular filtration [8,15]. Since the internalization of monomeric ADAPT6s is slow, strong residualizing properties of the label are not essential for retention of the activity shortly after injection (1–4 h after injection), but the use of a non-residualizing radioiodine label is more suitable since it enables decrease of the renal retention of radioactivity [16]. The results of the cellular processing experiments (Figs. 7 and 8) demonstrate that internalization of both radiolabelled dimeric forms is relatively slow and similar to internalization of the monomeric forms of ADAPT6 [15,16]. This is an essential feature of the dimeric ADAPTs, since bivalent binding other targeting proteins and peptides to a cell-surface target is often associated with a rapid internalization of a target-ligand complex due to the cross-linking effect [34,45–47]. The slow internalization of dimeric ADAPTs correlates well with the aforementioned 1:1 interaction, suggesting that there is no simultaneous binding to two cell-surface receptors and no cross-linking. The slow internalization of the dimeric forms of ADAPT6 enables the use of non-residualizing radiohalogen labels. Indeed, although both the internalized fraction and the overall cell-associated activity were lower for ^{125}I-HPEM-DiADAPT6L2 and ^{125}I-HPEM-DOTA-DiADAPT6L3 at 24 h compared to their ^{111}In-labeled counterparts, this effect was not very pronounced at 4 h, which is a relevant time point for in vivo imaging.

Animal studies confirmed that the radiolabelled dimeric forms of ADAPT6 are capable of specific targeting of HER2 expressing tumour xenografts *in vivo* (Fig. 9) and can provide high-contrast images of HER2-epressing xenografts. The difference in linker length did not result in significant difference in biodistribution or tumour-targeting properties (Table 4). However, the tumour uptake of the dimeric forms of ADAPT6 was significantly lower than the uptake of the monomeric form for both labels at both time points measured in this study. Besides, the clearance rate of the dimeric forms labelled with the radiometal was slower than the clearance of the monomer (Table 4). Therefore, the tumour-to-organ ratios for the monomeric ADAPT6 were appreciably higher than for the dimeric ones (Table 5). Thus, the monomer provides better imaging contrast and is therefore the preferable format for development of ADAPT6-based tumour-targeting probes. It has to be noted that the tumour-to-organ ratios for the ADAPT dimers were much higher than the tumour-to-organ ratios provided by radiolabelled anti-HER2 monoclonal antibodies [13]. Furthermore, dimerization of affibody molecules, another engineered scaffold protein, also resulted in decreased tumour uptake despite increased affinities [32,38,48]. However, it was not clear if this phenomenon was related to that particular scaffold protein. In addition, the cited studies used non-residualizing radiohalogen labels and there was no reliable method for measurement of the internalization at that time. Therefore, the results for the affibody molecules might be attributed to accelerated internalization of dimers and leakage of radiohalogens from tumours. This study has shown the same phenomenon for the ADAPT scaffold, and the results when using the residualizing radiometal label, excluded influence of dimeric binding on internalization and retention. Taken together with previous data, this study implies that increasing the affinity by dimerization is not the way to improve in vivo targeting of small engineered scaffold proteins. The possible reason for this might be that the larger size due to dimerization, hampers efficient extravasation of dimers into the extracellular space of the tumours. On the other hand, the blood clearance rate of ADAPT dimers is nearly as high as for the monomeric ADAPTs. This prevents a maintained concentration gradient between blood and tumours and consequently there will be a continuous flow of the probe from blood to tumours.

Such strong influence of the size of a small targeting protein might be considered as strange. It is known that the tumour vasculature is hyperpermeable and the size-dependent transfer through pores in the vessels might play a minor role. Indeed, the localization of intact antibodies in tumours (both specific and unspecific) can be explained by this hyperpermeability. However, the localization of smaller antibody fragments in tumours is rapider than localization of intact IgG reaching maximum within 24 h after injection [49,50]. Even smaller engineered scaffold proteins localize in tumours even rapider, within 60 min [8,51]. Taken together, this indicates that the size of targeting proteins is essential for efficient tumour uptake. This study suggests that this is true even for targeting proteins with the mass in the range of 6–12 kDa.

5. Conclusions

In conclusion, dimeric forms of ADAPT6 with optimal linker lengths have substantially higher affinity compared to the monomeric variant. However, the dimeric forms of ADAPT6 showed a lower tumour uptake compared to the monomeric variant. This suggests that affinity maturation would be the preferable way to increase affinity of tumour-targeting engineered scaffold proteins.

Acknowledgements

This research was financially supported by the Swedish Cancer Society [Grants CAN 2015/350 and 2017/425], the Swedish Research Council [Grants 2015-02353, 2015-02509], and the Swedish Agency for Innovation VINNOVA [Grant 2015-02509].

Competing interest statement

The authors have no competing interests to declare.

References

[1] D.A. Mankoff, C.E. Edmonds, M.D. Farwell, D.A. Pryma, Development of companion diagnostics, Semin. Nucl. Med. 46 (2016) 47–56, https://doi.org/10.1053/j.semnuclmed.2015.09.002.

[2] A. Krasniqi, M. D'Huyvetter, N. Devoogdt, F.Y. Frejd, J. Sörensen, A. Orlova, M. Keyaerts, V. Tolmachev, Same-day imaging using small proteins: clinical experience and translational prospects in oncology, J. Nucl. Med. 59 (2018) 885–891, https://doi.org/10.2967/jnumed.117.199901.

[3] H.-J. Wester, H. Kessler, Molecular targeting with peptides or peptide-polymer conjugates: just a question of size? J. Nucl. Med. 46 (2005) 1940–1945.

[4] J. Nilvebrant, S. Hober, The albumin-binding domain as a scaffold for protein engineering, Comput. Struct. Biotechnol. J. 6 (2013) e201303009, https://doi.org/10.5936/csbj.201303009.

[5] J. Nilvebrant, T. Alm, S. Hober, J. Löfblom, Engineering bispecificity into a single albumin-binding domain, PLoS ONE 6 (2011) e25791.

[6] J. Nilvebrant, M. Astrand, J. Löfblom, S. Hober, Development and characterization of small bispecific albumin-binding domains with high affinity for ErbB3, Cell. Mol. Life Sci. 70 (2013) 3973–3985, https://doi.org/10.1007/s00018-013-1370-9.

[7] J. Nilvebrant, M. Åstrand, M. Georgieva-Kotseva, M. Björnmalm, J. Löfblom, S. Hober, Engineering of bispecific affinity proteins with high affinity for ERBB2 and adaptable binding to albumin, PLoS ONE 9 (2014) e103094, https://doi.org/10.1371/journal.pone.0103094.

[8] J. Garousi, S. Lindbo, J. Nilvebrant, M. Åstrand, J. Buijs, M. Sandström, H. Honarvar, A. Orlova, V. Tolmachev, S. Hober, ADAPT, a novel scaffold protein-based probe for radionuclide imaging of molecular targets that are expressed in disseminated cancers, Cancer Res. 75 (2015) 4364–4371, https://doi.org/10.1158/0008-5472.CAN-14-3497.

[9] S.H. Giordano, S. Temin, N.E. Davidson, Systemic therapy for patients with advanced human epidermal growth factor receptor 2-positive breast cancer: ASCO Clinical Practice Guideline Update Summary, J. Oncol. Pract. (2018) JOP1800290, https://doi.org/10.1200/JOP.18.00290.

[10] J. Maresch, S.F. Schoppmann, C.M.R. Thallinger, C.C. Zielinski, M. Hejna, Her-2/neu gene amplification and over-expression in stomach and esophageal adenocarcinoma: from pathology to treatment, Crit. Rev. Oncol. Hematol. 82 (2012) 310–322, https://doi.org/10.1016/j.critrevonc.2011.06.003.

[11] A.C. Wolff, M.E.H. Hammond, D.G. Hicks, M. Dowsett, L.M. McShane, K.H. Allison, D.C. Allred, J.M.S. Bartlett, M. Bilous, P. Fitzgibbons, W. Hanna, R.B. Jenkins, P.B. Mangu, S. Paik, E.A. Perez, M.F. Press, P.A. Spears, G.H. Vance, G. Viale, D.F. Hayes, American Society of Clinical Oncology, College of American Pathologists, Recommendations for human epidermal growth factor receptor 2 testing in breast cancer: American Society of Clinical Oncology/College of American Pathologists clinical practice guideline update, J. Clin. Oncol. 31 (2013) 3997–4013, https://doi.org/10.1200/JCO.2013.50.9984.

[12] N.A.C.S. Wong, F. Amary, R. Butler, R. Byers, D. Gonzalez, H.R. Haynes, M. Ilyas, M. Salto-Tellez, P. Taniere, HER2 testing of gastro-oesophageal adenocarcinoma: a commentary and guidance document from the Association of Clinical Pathologists Molecular Pathology and Diagnostics Committee, J. Clin. Pathol. 71 (2018) 388–394, https://doi.org/10.1136/jclinpath-2017-204943.

[13] V. Tolmachev, Imaging of HER-2 overexpression in tumors for guiding therapy, Curr. Pharm. Des. 14 (2008) 2999–3019.

[14] S. Lindbo, J. Garousi, M. Åstrand, H. Honarvar, A. Orlova, S. Hober, V. Tolmachev, Influence of histidine-containing tags on the biodistribution of ADAPT scaffold proteins, Bioconjug. Chem. 27 (2016) 716–726, https://doi.org/10.1021/acs.bioconjchem.5b00677.

[15] J. Garousi, S. Lindbo, H. Honarvar, J. Velletta, B. Mitran, M. Altai, A. Orlova, V. Tolmachev, S. Hober, Influence of the N-Terminal composition on targeting properties of radiometal-labeled anti-HER2 scaffold protein ADAPT6, Bioconjug. Chem. 27 (2016) 2678–2688, https://doi.org/10.1021/acs.bioconjchem.6b00465.

[16] J. Garousi, S. Lindbo, B. Mitran, J. Buijs, A. Vorobyeva, A. Orlova, V. Tolmachev, S. Hober, Comparative evaluation of tumor targeting using the anti-HER2 ADAPT scaffold protein labeled at the C-terminus with indium-111 or technetium-99m, Sci Rep. 7 (2017) 14780, https://doi.org/10.1038/s41598-017-15366-w.

[17] S. Lindbo, J. Garousi, B. Mitran, M. Altai, J. Buijs, A. Orlova, S. Hober, V. Tolmachev, Radionuclide tumor targeting using ADAPT scaffold proteins: aspects of label positioning and residualizing properties of the label, J. Nucl. Med. 59 (2018) 93–99, https://doi.org/10.2967/jnumed.117.197202.

[18] S. Lindbo, J. Garousi, B. Mitran, A. Vorobyeva, M. Oroujeni, A. Orlova, S. Hober, V. Tolmachev, Optimized molecular design of ADAPT-based HER2-imaging probes labeled with 111In and 68Ga, Mol. Pharm. 15 (2018) 2674–2683, https://doi.org/10.1021/acs.molpharmaceut.8b00204.

[19] V. Tolmachev, T.A. Tran, D. Rosik, A. Sjöberg, L. Abrahmsén, A. Orlova, Tumor targeting using affibody molecules: interplay of affinity, target expression level, and binding site composition, J. Nucl. Med. 53 (2012) 953–960, https://doi.org/10.2967/jnumed.111.101527.

[20] S. Minner, B. Jessen, L. Stiedenroth, E. Burandt, J. Köllermann, M. Mirlacher, A. Erbersdobler, C. Eichelberg, M. Fisch, T.H. Brümmendorf, C. Bokemeyer, R. Simon, T. Steuber, M. Graefen, H. Huland, G. Sauter, T. Schlomm, Low level HER2 overexpression is associated with rapid tumor cell proliferation and poor prognosis in prostate cancer, Clin. Cancer Res. 16 (2010) 1553–1560, https://doi.org/10.1158/1078-0432.CCR-09-2546.

[21] J.S. Ross, J.A. Fletcher, The HER-2/neu oncogene in breast cancer: prognostic factor, predictive factor, and target for therapy, Oncologist 3 (1998) 237–252.

[22] L. Cao, Y. Yu, I. Darko, D. Currier, L.H. Mayeenuddin, X. Wan, C. Khanna, L.J. Helman, Addiction to elevated insulin-like growth factor I receptor and initial modulation of the AKT pathway define the responsiveness of rhabdomyosarcoma to the targeting antibody, Cancer Res. 68 (2008) 8039–8048.

[23] J. Zha, C. O'Brien, H. Savage, L.-Y. Huw, F. Zhong, L. Berry, G.D. Lewis Phillips, E. Luis, G. Cavet, X. Hu, L.C. Amler, M.R. Lackner, Molecular predictors of response to a humanized anti-insulin-like growth factor-I receptor monoclonal antibody in breast and colorectal cancer, Mol. Cancer Ther. 8 (2009) 2110–2121, https://doi.org/10.1158/1535-7163.MCT-09-0381.

[24] M. Rosestedt, K.G. Andersson, B. Mitran, V. Tolmachev, J. Löfblom, A. Orlova, S. Ståhl, Affibody-mediated PET imaging of HER3 expression in malignant tumours, Sci Rep. 5 (2015) 15226, https://doi.org/10.1038/srep15226.

[25] A. Orlova, M. Magnusson, T.L.J. Eriksson, M. Nilsson, B. Larsson, I. Höidén-Guthenberg, C. Widström, J. Carlsson, V. Tolmachev, S. Ståhl, F.Y. Nilsson, Tumor imaging using a picomolar affinity HER2 binding affibody molecule, Cancer Res. 66 (2006) 4339–4348, https://doi.org/10.1158/0008-5472.CAN-05-3521.

[26] M. Friedman, A. Orlova, E. Johansson, T.L.J. Eriksson, I. Höidén-Guthenberg, V. Tolmachev, F.Y. Nilsson, S. Ståhl, Directed evolution to low nanomolar affinity of a tumor-targeting epidermal growth factor receptor-binding affibody molecule, J. Mol. Biol. 376 (2008) 1388–1402, https://doi.org/10.1016/j.jmb.2007.12.060.

[27] I. Dijkgraaf, C.-B. Yim, G.M. Franssen, R.C. Schuit, G. Luurtsema, S. Liu, W.J.G. Oyen, O.C. Boerman, PET imaging of $\alpha v\beta_3$ integrin expression in tumours with ^{68}Ga-labelled mono-, di- and tetrameric RGD peptides, Eur. J. Nucl. Med. Mol. Imaging 38 (2011) 128–137, https://doi.org/10.1007/s00259-010-1615-x.

[28] N. Guo, L. Lang, H. Gao, G. Niu, D.O. Kiesewetter, Q. Xie, X. Chen, Quantitative analysis and parametric imaging of 18F-labeled monomeric and dimeric RGD peptides using compartment model, Mol Imaging Biol. 14 (2012) 743–752, https://doi.org/10.1007/s11307-012-0541-7.

[29] Z. Wu, S. Liu, I. Nair, K. Omori, S. Scott, I. Todorov, J.E. Shively, P.S. Conti, Z. Li, F. Kandeel, (64)Cu labeled sarcophagine exendin-4 for microPET imaging of glucagon like peptide-1 receptor expression, Theranostics 4 (2014) 770–777, https://doi.org/10.7150/thno.7759.

[30] G.P. Adams, M.-S. Tai, J.E. McCartney, J.D. Marks, W.F. Stafford, L.L. Houston, J.S. Huston, L.M. Weiner, Avidity-mediated enhancement of in vivo tumor targeting by single-chain Fv dimers, Clin. Cancer Res. 12 (2006) 1599–1605.

[31] A.-C. Steffen, M. Wikman, V. Tolmachev, G.P. Adams, F.Y. Nilsson, S. Ståhl, J. Carlsson, In vitro characterization of a bivalent anti-HER-2 affibody with potential for radionuclide-based diagnostics, CancerBiother. Radiopharm. 20 (2005) 239–248, https://doi.org/10.1089/cbr.2005.20.239.

[32] V. Tolmachev, M. Friedman, M. Sandström, T.L.J. Eriksson, D. Rosik, M. Hodik, S. Ståhl, F.Y. Frejd, A. Orlova, Affibody molecules for epidermal growth factor receptor targeting in vivo: aspects of dimerization and labeling chemistry, J. Nucl. Med. 50 (2009) 274–283, https://doi.org/10.2967/jnumed.108.055525.

[33] J.M. Hexham, D. Dudas, R. Hugo, J. Thompson, V. King, C. Dowling, D.M. Neville, M.E. Digan, P. Lake, Influence of relative binding affinity on efficacy in a panel of anti-CD3 scFv immunotoxins, Mol. Immunol. 38 (2001) 397–408.

[34] A. Krasniqi, M. Bialkowska, C. Xavier, K. Van der Jeught, S. Muyldermans, N. Devoogdt, M. D'Huyvetter, Pharmacokinetics of radiolabeled dimeric sdAbs constructs targeting human CD20, N Biotechnol. 45 (45) (2018) 69–79, https://doi.org/10.1016/j.nbt.2018.03.004.

[35] F. Fleetwood, R. Güler, E. Gordon, S. Ståhl, L. Claesson-Welsh, J. Löfblom, Novel affinity binders for neutralization of vascular endothelial growth factor (VEGF) signaling, Cell Mol Life Sci. 73 (2016) 1671–1683, https://doi.org/10.1007/s00018-015-2088-7.

[36] H. Lindberg, T. Härd, J. Löfblom, S. Ståhl, A truncated and dimeric format of an Affibody library on bacteria enables FACS-mediated isolation of amyloid-beta aggregation inhibitors with subnanomolar affinity, Biotechnol. J. 10 (2015) 1707–1718, https://doi.org/10.1002/biot.201500131.

[37] S.J. Hosseinimehr, V. Tolmachev, A. Orlova, Liver uptake of radiolabeled targeting proteins and peptides: considerations for targeting peptide conjugate design, Drug Discov Today 17 (21–22) (2012) 1224–1232.

[38] V. Tolmachev, E. Mume, S. Sjöberg, F.Y. Frejd, A. Orlova, Influence of valency and labelling chemistry on in vivo targeting using radioiodinated HER2-binding Affibody molecules, Eur. J. Nucl. Med. Mol. Imaging 36 (2009) 692–701, https://doi.org/10.1007/s00259-008-1003-y.

[39] E. Mume, A. Orlova, B. Larsson, A.-S. Nilsson, F.Y. Nilsson, S. Sjöberg, V. Tolmachev, Evaluation of ((4-hydroxyphenyl)ethyl)maleimide for site-specific radiobromination of anti-HER2 affibody, Bioconjug. Chem. 16 (2005) 1547–1555, https://doi.org/10.1021/bc050056o.

[40] H. Wållberg, A. Orlova, Slow internalization of anti-HER2 synthetic affibody monomer 111In-DOTA-ZHER2:342-pep2: implications for development of labeled tracers, CancerBiother. Radiopharm. 23 (2008) 435–442, https://doi.org/10.1089/cbr.2008.0464.

[41] H. Björkelund, L. Gedda, P. Barta, M. Malmqvist, K. Andersson, Gefitinib induces

epidermal growth factor receptor dimers which alters the interaction characteristics with 125I-EGF, PLoS One 6 (2011) e24739.
[42] M.M. Schmidt, K.D. Wittrup, A modeling analysis of the effects of molecular size and binding affinity on tumor targeting, Mol. Cancer Ther. 8 (2009) 2861–2871, https://doi.org/10.1158/1535-7163.MCT-09-0195.
[43] E.W. Price, C. Orvig, Matching chelators to radiometals for radiopharmaceuticals, Chem. Soc. Rev. 43 (2014) 260–290, https://doi.org/10.1039/c3cs60304k.
[44] V. Tolmachev, A. Orlova, Influence of labelling methods on biodistribution and imaging properties of radiolabelled peptides for visualisation of molecular therapeutic targets, Curr. Med. Chem. 17 (2010) 2636–2655.
[45] R.M. Hudziak, G.D. Lewis, M. Winget, B.M. Fendly, H.M. Shepard, A. Ullrich, p185HER2 monoclonal antibody has antiproliferative effects in vitro and sensitizes human breast tumor cells to tumor necrosis factor, Mol. Cell. Biol. 9 (1989) 1165–1172.
[46] J.K. Sosabowski, T. Matzow, J.M. Foster, C. Finucane, D. Ellison, S.A. Watson, S.J. Mather, Targeting of CCK-2 receptor-expressing tumors using a radiolabeled divalent gastrin peptide, J. Nucl. Med. 50 (2009) 2082–2089, https://doi.org/10.2967/jnumed.109.064808.
[47] A. Vaidyanath, T. Hashizume, T. Nagaoka, N. Takeyasu, H. Satoh, L. Chen, J. Wang, T. Kasai, T. Kudoh, A. Satoh, L. Fu, M. Seno, Enhanced internalization of ErbB2 in SK-BR-3 cells with multivalent forms of an artificial ligand, J. Cell. Mol. Med. 15 (2011) 2525–2538, https://doi.org/10.1111/j.1582-4934.2011.01277.x.
[48] Z. Cheng, O.P. De Jesus, M. Namavari, A. De, J. Levi, J.M. Webster, R. Zhang, B. Lee, F.A. Syud, S.S. Gambhir, Small-animal PET imaging of human epidermal growth factor receptor type 2 expression with site-specific 18F-labeled protein scaffold molecules, J. Nucl. Med. 49 (2008) 804–813, https://doi.org/10.2967/jnumed.107.047381.
[49] P.M. Smith-Jones, D.B. Solit, T. Akhurst, F. Afroze, N. Rosen, S.M. Larson, Imaging the pharmacodynamics of HER2 degradation in response to Hsp90 inhibitors, Nat. Biotechnol. 22 (2004) 701–706, https://doi.org/10.1038/nbt968.
[50] V. Kenanova, A.M. Wu, Tailoring antibodies for radionuclide delivery, Expert Opin. Drug Deliv. 3 (2006) 53–70, https://doi.org/10.1517/17425247.3.1.53.
[51] S. Ahlgren, A. Orlova, H. Wållberg, M. Hansson, M. Sandström, R. Lewsley, A. Wennborg, L. Abrahmsén, V. Tolmachev, J. Feldwisch, Targeting of HER2-expressing tumors using 111In-ABY-025, a second-generation affibody molecule with a fundamentally reengineered scaffold, J. Nucl. Med. 51 (2010) 1131–1138, https://doi.org/10.2967/jnumed.109.073346.